

Sensitivity of solar f-mode travel times to internal flows

Jason Jackiewicz and Laurent Gizon

Max Planck Institut für Sonnensystemforschung, Katlenburg-Lindau, 37191, Germany

Aaron C. Birch

Colorado Research Associates, a Division of Northwest Research Associates Inc., Boulder, CO, 80301, USA

We compute f-mode travel-time sensitivity kernels for flows. Using a two-dimensional model, we show that it is important to account for several systematic effects, such as the foreshortening and the projection of the velocity vector onto the line of sight. Correcting for these effects is necessary before any data inversion is attempted away from the center of the solar disk.

I. INTRODUCTION

The solar f-modes are useful tools for studying perturbations that reside within the top 2 Mm of the surface of the Sun, and have been used as a diagnostic as such before, e.g., Duvall & Gizon [2]. The linear forward problem of time-distance helioseismology is to calculate functions, or kernels, which give the sensitivity of travel-time measurements to these particular perturbations of the f-modes. For a discussion of this general procedure, which is the one that we will follow here, see Gizon & Birch [3].

In this study we are interested in *flow* kernels, i.e., functions which give the two-dimensional sensitivity of travel-time measurements to small amplitude, two-dimensional, spatially varying flows. The flow kernel, \mathbf{K} , is defined as

$$\delta\tau = \iint_S d^2\mathbf{r} \mathbf{u}(\mathbf{r}) \cdot \mathbf{K}(\mathbf{r}), \quad (1)$$

where $\delta\tau$ is the perturbation to the travel time, $\mathbf{u} = (u_x, u_y)$ is the two-dimensional flow perturbation, and the integral is over the position vector $\mathbf{r} = (x, y)$ over the whole solar surface. The kernel $\mathbf{K} = (K_x, K_y)$ is a two-dimensional vector which has sensitivity to flows in the x and y directions.

We calculate the kernels from an approximate solar model, which utilizes the Born approximation in estimating the scattering from solar inhomogeneities. This has been shown to be more accurate than calculating kernels from a ray approximation [1], since it includes finite-wavelength effects.

Ultimately, the goal is to perform inversions with real time-distance measurements to extract the unknown \mathbf{u} from Eq.(1), given $\delta\tau$ and \mathbf{K} . However, there are several difficulties in doing this since the travel-time measurements incur systematic effects from the observing process, particularly due to the center-to-limb variations. To overcome these problems, one strategy is to calculate the sensitivity kernels from the outset accounting for the systematic effects so that the whole procedure - the forward calculation and the inversions - remains consistent.

We have accomplished this for two important effects: the foreshortening of the data pixel, and the projection of the solar velocity field onto the line of sight, both of which will be defined in detail below. We present an analysis of the contribution that these two effects have on the power spectrum of f-modes and on the kernels. For brevity, we leave the details of the full calculation of the power spectra and kernels for a

future publication [4], and only focus here on the role of the systematic effects mentioned above on the final results.

II. MODEL POWER SPECTRUM

A. Line of sight projection

A local region of the Sun may be approximated by a plane which is tangent to the sphere. The orientation of the normal to the plane with respect to the observer depends on the position on the sphere on which this plane lies. We denote the line of sight unit vector, $\hat{\ell} = (\hat{\ell}_h, \ell_z)$, as the direction which points towards the observer from the point where the plane intersects the sphere. In this notation, $\ell_z = 1$ only at the disk center. Doppler measurements of oscillation velocities \mathbf{v} on the Sun return the projection of \mathbf{v} onto $\hat{\ell}$. For the purpose of inversions, in order to have confidence in utilizing all of the data from instruments such as MDI and HMI, even data well away from disk center, the sensitivity kernels in principle should account for a changing $\hat{\ell}$, as to avoid the aforementioned inherent systematic errors. In the past, kernels have been calculated only with $\ell_z = 1$ as a first attempt. We calculate kernels here for any $\hat{\ell}$.

In general, the observable oscillation signal, $\psi(\mathbf{r}, t)$, can be written as

$$\psi(\mathbf{r}, t) = \mathcal{F} \left\{ \hat{\ell}(\mathbf{r}) \cdot \mathbf{v}(\mathbf{r}, t) \right\}. \quad (2)$$

The operator \mathcal{F} involves the filtering procedure of the data, such as the time duration of the measurement, instrumental effects such as the MTF and the foreshortening, and possibly some phase speed filter. Using a similar model for f-modes as in Gizon & Birch [3], and similar notation, we calculate an expression for $\mathbf{v}(\mathbf{r}, t)$. The zero-order power spectrum of ψ (in the absence of a flow) can then be written for horizontal wavenumber \mathbf{k} and angular frequency ω as

$$P(\mathbf{k}, \omega) = (2\pi)^6 |\mathcal{G}(\mathbf{k}, \omega)|^2, \quad (3)$$

where

$$\mathcal{G}(\mathbf{k}, \omega) = \left(i\hat{\ell}_h \cdot \mathbf{k} + \ell_z \kappa(\omega) \right) \sqrt{m_s(\omega)} G(k, \omega) F(\mathbf{k}, \omega). \quad (4)$$

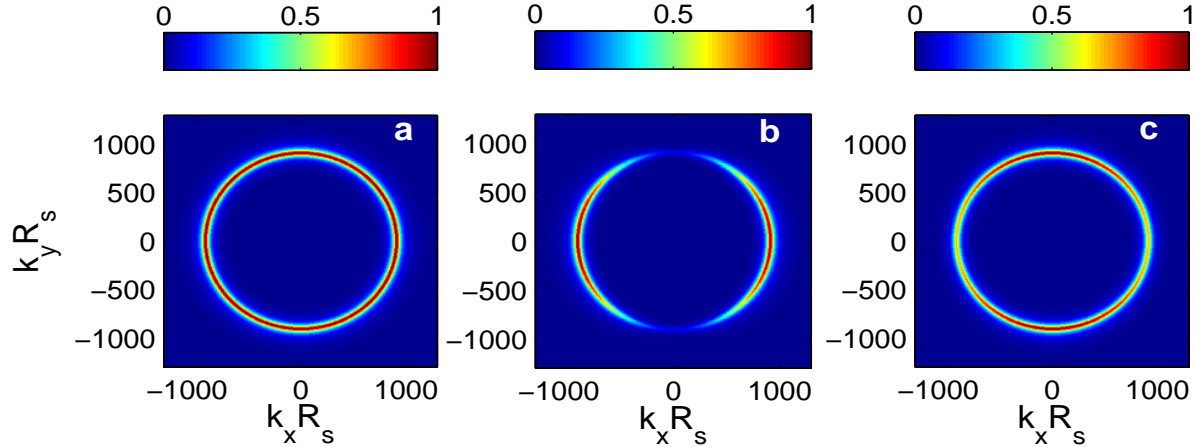


FIG. 1: A cut in three different power spectra at constant $\omega/2\pi = 3$ mHz with $\Theta = 90^\circ$, where the x and y axes are in units of harmonic degree. (a) shows the power at the disk center ($\Phi = 0$) for reference. (b) is the power at $\Phi = 75^\circ$, with the effect of the line of sight only (no foreshortening). (c) is again at $\Phi = 75^\circ$, but with the effect of foreshortening included (no line of sight effect). All figures have been normalized by their maximum values, and $R_s = 696Mm$. We use a pixel size of an MDI hi-res image, $dx = 0.43$ Mm (see section II B).

Here, κ describes the frequency dependent damping, m_s is the source power, G is the Green's function, and F is a function that describes the effect of the filter operator \mathcal{F} mentioned above. For the purposes here, the important thing to note is the explicit dependence of the power on the line of sight vector, which is given as $\hat{\ell} = (-\sin \Phi, -\cos \Theta \cos \Phi, \sin \Theta \cos \Phi)$, where Φ , the solar longitude, is measured from the central meridian, and Θ is the co-latitude measured from the solar north pole. In our local plane coordinates, Φ is along \hat{x} , and Θ is along $-\hat{y}$.

Consider the power along the equator (Φ varies, Θ fixed at 90°), and without any foreshortening effects for now. Upon close inspection of Eq.(4), one sees that the magnitude of the power along the k_x direction is mostly unaffected, while the power along k_y is reduced. This is shown in Fig. 1, where we plot cuts at constant angular frequency in the power spectrum. The first panel, Fig. 1a, is at disk center, a reference plot where $\hat{\ell} = \hat{\ell}_z$. Fig. 1b is a power cut at $\Phi = 75^\circ$ towards the western limb, on the equator. As stated above, the power is reduced along the k_y direction.

To see this effect even more clearly, Fig. 2 is a plot of a cut in the power spectrum at constant ω for 4 different positions on the disk at fixed $|\mathbf{k}|$, versus the direction of $\hat{\mathbf{k}}$ (denoted by the angle θ_k that \mathbf{k} makes with the x axis), neglecting for the moment foreshortening effects. One sees that the power is always reduced along k_y with respect to the value at the disk center. The power along k_x is independent of Φ when only line of sight effects are considered.

Physically, we can understand this by considering the extreme case when we observe at the limb, on the equator. Waves that travel north-south will be undetectable because the motion is perpendicular to the line of sight, while waves that travel along the equatorial plane still give power.

B. Foreshortening

Foreshortening occurs due to the fact that the spatial resolution (measured on the Sun) decreases as we observe toward the limb. After projection onto the local plane, a ccd pixel will then appear elongated in the center-to-limb direction. Again, consider a region towards the limb on the equator. A pixel that has a horizontal resolution of dx at disk center, now images a horizontal distance on the Sun of dx/μ , where $\mu = \cos \Phi \sin \Theta$. This reduces the effective spatial resolu-

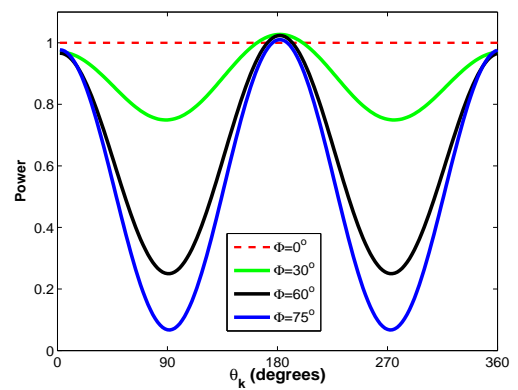


FIG. 2: Power in normalized units versus θ_k for the 4 different values of Φ along the equator ($\Theta = 90^\circ$), given in the legend. Here, $\ell = 900$ and $\omega/2\pi = 3$ mHz, corresponding to the power maximum of the f-mode. Note how only along k_y ($\theta_k = 90^\circ, \theta_k = 270^\circ$) does the power get reduced due to the line of sight projection. Each curve is divided by the power at disk center (red dashed line) for normalization.

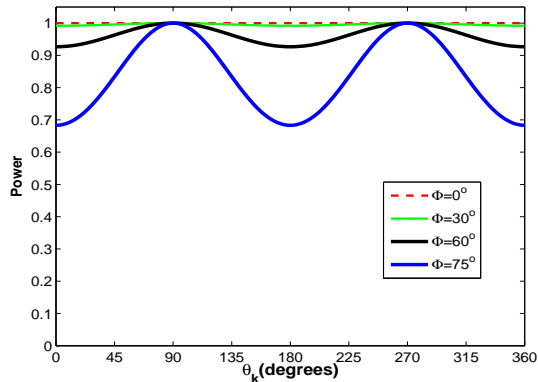


FIG. 3: Same as in Fig. 2 with all curves at $\Theta = 90^\circ$, but now we show the power taking into account the foreshortening $\Lambda(\mathbf{k})$ without any line of sight effects. Note how the foreshortening is $\pi/2$ out of phase with the line of sight (compare with Fig. 2).

tion measured on the Sun in the center-to-limb direction, and hence leads to systematic observational errors.

To correct for this, we return to the expressions for the power given above in Eqs.(3,4). The filter function $F(\mathbf{k}, \omega)$ contains the information about the foreshortening. We break the filter into its constituent parts, and rewrite it as

$$F(\mathbf{k}, \omega) = f(k, \omega)\Lambda(\mathbf{k}), \quad (5)$$

where the lowercase $f(k, \omega)$ contains the MTF and/or other filters, which only depend on k , and $\Lambda(\mathbf{k})$ is the foreshortening correction. For the sake of simplicity, we obtain $\Lambda(\mathbf{k})$ by taking the Fourier transform of an elliptical disk, which is approximately the projection of a ccd pixel onto the local plane. We require that the ellipse only gets elongated along the center-to-limb direction, which is always along the semi-major axis. The semi-minor axis stays at fixed length. Carrying out this integration gives a term proportional to a Bessel function of first order. Expanding the Bessel function in a small parameter k (wavenumber) results in an expression given as

$$\Lambda(\mathbf{k}) \approx \Lambda_0(k) + \Lambda_1(k) \sin^2(\theta_k - \alpha), \quad (6)$$

where $\Lambda_0(k)$ and $\Lambda_1(k)$ are only functions of k and are of little interest here, except to note that they depend on the eccentricity of the ellipse, and hence on Θ and Φ . We denote by α the angle which describes the orientation of the ellipse on the disk. More precisely, it is the angle that the semi-major axis of the ellipse makes with a local latitude line, and is also a function of Θ and Φ . All of the other details of this calculation are beyond the scope of this paper, and will be presented elsewhere.

The foreshortening term (6) now can be inserted into the power to study its effects. Returning to Fig. 1, in panel (c) we plot the power including the foreshortening function, but this time neglecting the line of sight effect. We see that the foreshortening effect is 90 degrees out of phase with the line of sight effect from panel Fig. 1b. The power is reduced instead

along the k_x direction. We can understand this physically, because waves are attenuated at high wavenumber, due to the smaller pixel size in Fourier space in the center-to-limb direction.

As was done for the line of sight case, we show a cut of the power at $\ell = 900$, $\omega/2\pi = 3$ mHz versus θ_k in Fig. 3 to see the reduced power in the k_x direction more clearly as the limb is approached. This figure, along with Fig. 2, demonstrates that the net reduction of power is always larger due to line of sight effects, i.e., at $\Phi = 75^\circ$, the power is only about 10 % of its disk center value along k_y , while it is still about 70 % of its disk center value along k_x . The evidence for this is also in Fig. 1b, where the power is almost gone along k_y , but is still somewhat present in panel (c) along k_x .

III. KERNELS

We calculate the flow kernels \mathbf{K} based on the general method described in Gizon & Birch [3], where kernels were calculated only for damping and source perturbations to f-modes. The flow kernels here are computed in a completely analogous manner: we use the single-scattering Born approximation. The effects of the line of sight and foreshortening are explicitly included in the calculation.

Since we are interested in detecting flows, we consider travel-time *differences* between two points on the Sun. Because waves that travel in the direction of a flow travel faster than they would against it, this definition of travel time difference is sensible for extracting flows. In Fig. 4 we plot kernels for travel-time differences that are sensitive to flows travelling in the $+\hat{x}$ direction (K_x), where the two observation points are given by the left and right crosses. Fig. 4a is computed for the center of the grid at disk center. For flow perturbations between the observation points (blue region), one sees a negative value of the kernel, as expected. In other areas, wave effects produce non-trivial behavior. Fig. 4b, computed well towards the western limb, demonstrates how the line of sight and foreshortening effects alter the kernel, as does Fig. 4c, which is a plot of a kernel on the central meridian at $\Theta = 15^\circ$. The kernel in Fig. 4c shows quite different structure, in fact, it has very little sensitivity along the line connecting the two observation points; only waves that scatter off of the unperturbed ray path can be detected. The decomposition of the sensitivity kernel into Fresnel zones (e.g. Jensen [5]) is not obvious in this last example. Also, note that even though the integral over space of the three kernels in Fig. 4 is approximately the same, the spatial-dependence is quite different, and an inversion using these kernels would give different results for flows varying on a scale comparable to or smaller than the wavelength of f-modes.

IV. CONCLUSIONS

We have calculated sensitivity kernels for flows for time-distance helioseismology. The effects of the line of sight and the foreshortening, as defined above, have been demonstrated

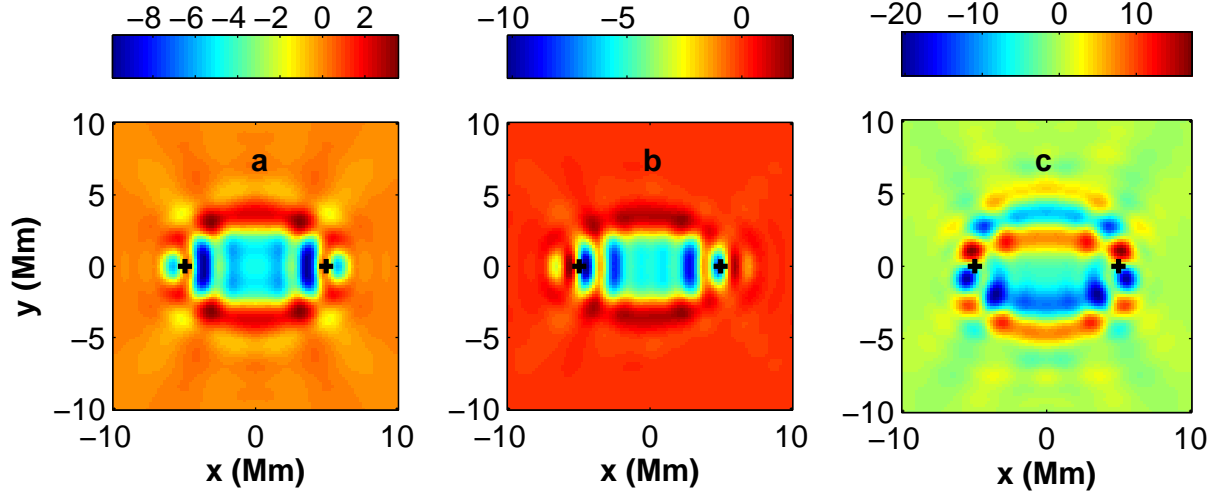


FIG. 4: F-mode sensitivity kernels K_x for flows in the $+\hat{x}$ direction. (a) is calculated at disk center ($\Phi = 0$, $\Theta = 90^\circ$), (b) for $\Phi = 75^\circ$, $\Theta = 90^\circ$, and (c) for $\Phi = 0$, $\Theta = 15^\circ$. The crosses at $r_1 = (-5, 0)$ Mm, $r_2 = (5, 0)$ Mm denote the two observation points. The units of the colorscale are $s(km/s)^{-1}Mm^{-2}$. Note that the integral over space of each kernel is approximately the same.

for a model power spectrum and the kernels. The next step is to study real data for f modes to compare the observed power

spectra with the modeled ones to gain confidence in our theoretical sensitivity kernels.

-
- [1] Birch A.C. and Felder G., 2004, ApJ 616, 1261
 [2] Duvall Jr. T.L. and L. Gizon, 2000, Sol. Phys. 192, 177
 [3] Gizon L. and Birch A.C., 2002, ApJ 571, 966

- [4] Jackiewicz J., Gizon L., and Birch A.C., 2006, in preparation
 [5] Jensen, J.M., 2001, Ph.D. Thesis, Aarhus University